SANDIA REPORT
SAND2014-18179
Unlimited Release
Printed Month and Year

A New Maximum-Likelihood Change Estimator for Two-Pass SAR Coherent Change Detection

Daniel E. Wahl, David A. Yocky, and Charles V. Jakowatz, Jr.

Prepared by
Sandia National Laboratories
Albuquerque, New Mexico 87185 and Livermore, California 94550

Sandia National Laboratories is a multi-program laboratory managed and operated by Sandia Corporation, a wholly owned subsidiary of Lockheed Martin Corporation, for the U.S. Department of Energy's National Nuclear Security Administration under contract DE-AC04-94AL85000.

Issued by Sandia National Laboratories, operated for the United States Department of Energy by Sandia Corporation.

Available to DOE and DOE contractors from
U.S. Department of Energy
Office of Scientific and Technical Information
P.O. Box 62
Oak Ridge, TN 37831

Telephone: (865) 576-8401
Facsimile: (865) 576-5728
E-Mail: reports@adonis.osti.gov
Online ordering: http://www.osti.gov/bridge

Available to the public from
U.S. Department of Commerce
National Technical Information Service
5285 Port Royal Rd.
Springfield, VA 22161

Telephone: (800) 553-6847
Facsimile: (703) 605-6900
E-Mail: orders@ntis.fedworld.gov
Online order: http://www.ntis.gov/help/ordermethods.asp?loc=7-4-0#online

SAND200X-XXXX
Unlimited Release
Printed Month Year

A New Maximum-Likelihood Change Estimator for Two-Pass SAR Coherent Change Detection

Daniel E. Wahl, David A. Yocky, and Charles V. Jakowatz, Jr.
Signal Processing & Technology Department
Sandia National Laboratories
P.O. Box 5800
Albuquerque, New Mexico 87185-MS1207

Abstract

In this paper, we derive a new optimal change metric to be used in synthetic aperture RADAR (SAR) coherent change detection (CCD). Previous CCD methods tend to produce false alarm states (showing change when there is none) in areas of the image that have a low clutter-to-noise power ratio (CNR). The new estimator does not suffer from this shortcoming. It is a surprisingly simple expression, easy to implement, and is optimal in the maximum-likelihood (ML) sense. The estimator produces very impressive results on the CCD collects that we have tested.

ACKNOWLEDGMENTS

The authors thank Robert Riley for collecting and supplying FARAD X-band complex-valued SAR imagery to us. This research was supported by DOE NA-22 (Defense Nuclear Nonproliferation Research and Development, Office of Proliferation Detection / Enabling Capabilities) under the direction of Dr. Victoria Franques. Sandia National Laboratories is a multi-program laboratory operated by the Sandia Corporation, a wholly owned subsidiary of Lockheed Martin Corporation, for the United States Department of Energy's National Nuclear Security Administration under contract DE-AC04-94AL85000.

CONTENTS

FIGURES

NOMENCLATURE

CCD	coherent change detection
CNR	clutter-to-noise power ratio
dB	decibel
DOE	Department of Energy
IID	independent identically distributed
ML	maximum likelihood
SAR	synthetic aperture RADAR
SNL	Sandia National Laboratories

[This page intentionally blank]

1. INTRODUCTION

Synthetic aperture radar (SAR) coherent change detection (CCD) was first proposed to detect anthropogenic and zoogenic temporal changes by Jakowatz et al. in 1996 using repeat-pass, repeat-geometry SAR collections [1]. At the time, most repeat-pass, repeat-geometry, coherent SAR collections were being exploited as interferometric SAR image pairs for terrain height measures using the interferometric fringe pattern between complex images [2, 3, 4, 5, 6, 7, 8]. Interferometric SAR research showed that the quality of interference fringes, which represent the phase difference between images, improves with the magnitude of the complex correlation coefficient, also called the degree of coherence [9, 6]. It is defined as

$$\alpha = \frac{\left| \sum_{k=1}^{N} X_{1k}^{*} X_{2k} \right|}{\sqrt{\sum_{k=1}^{N} |X_{1k}|^2 \sum_{k=1}^{N} |X_{2k}|^2}} \qquad (1)$$

where X_{1k} and X_{2k} represent the k^{th} complex values of image 1 and image 2 respectively, the * symbol denotes the complex conjugate operation, and α is the estimated change metric. The summation in Equation 1 occurs over a neighborhood (also called a "box" or "window") of image samples, with N the number of samples in the window and generally known as the "number of looks." In practice, neighborhood box sizes range from 3 x 3 to 9 x 9, but are not limited to square dimensions. For example, a 3 x 3 box results in 9 looks while a 9 x 9 box results in 81 looks.

If two noiseless SAR images are collected from precisely the same collection geometry at different times, and the surface microwave reflectivity does not change anywhere in the scene over this time period, the quantity α of Equation 1 produces a value of unity everywhere. Unfortunately, exact repeat geometry is difficult to achieve, not all targets reflect SAR wavelengths well, system thermal noise exists, and temporal reflectance change can occur. All of these factors can lead to reduced complex correlation [10].

The essential notion of CCD is to detect only the temporal reflectance changes that occur between pass 1 and pass 2 while minimizing the other effects that may cause low decorrelation. Detection of temporal reflectance changes occurring between the two SAR collections can be of value to the mission of the SAR system. These detections can be a result of subtle physical changes on the earth surface. For example, vehicles that randomize the surface reflectance where they travel (e.g. on dirt roads) can be detected as a local loss of the coherence measure [1, 11]. In addition, this methodology turns out to be sufficiently sensitive to indicate human bipedal travel [12].

In Jakowatz et al.'s presentation of CCD [1], they derived the repeat collection geometry constraints for successful pair processing and showed the optimal change estimator to be the coherence measure given in Equation 1. However, this estimator is optimal only when two

conditions exist: 1) The power in the two images is approximately equal; and 2) the CNR throughout the scene is very large. CNR is the clutter-to-noise ratio and is defined as:

$$\mathrm{CNR} = \frac{\sigma_c^2}{\sigma_n^2} \tag{2}$$

where σ_c^2 is the clutter power (signal power reflected by the clutter of the scene in a given neighborhood image pixels) and σ_n^2 is the noise power in the same window.

The statistical performance of Equation 1's change estimator has been extensively studied [13, 14], and it is well known that in situations where the CNR is low, the estimator is biased and would indicate that a change has occurred when it did not (producing a false alarm condition). Decorrelation due to low CNR can occur for many features in the SAR scene, including hard-packed roads or other smooth surfaces, shadowed areas, smooth water surfaces, and materials that have low radar reflectivities for various reasons.

Several methods have been proposed to overcome false alarms (change decorrelation) due to low CNR imagery values rather than true temporal changes. Some authors suggest using CNR information from the SAR imagery pair to mask areas that may produce false alarms [12]. Another technique uses three or more passes [15]. Here the CCD result from passes 1 and 2 is assumed to capture a "no-change" state, providing a change map with which to compare subsequent CCD results. This technique requires more than two passes and assumes that no changes have occurred between the two passes that provide the "no-change" state. Other authors propose a detection/estimation solution by developing a two-class (change or no-change) state. The results of this approach produce a log-likelihood value based on the measured data [16, 17].

Previous research attempts to correct the false change deficiencies of Equation 1 by post processing methods. We take a different approach. We revisit the maximum-likelihood derivation developed in [1] and re-derive the change metric in full rigor without the simplifying assumption of large CNR. The final result from this approach is a new, general maximum-likelihood estimator of the two-pass change statistic that should replace the traditional coherence measure of Equation 1 for CCD generation.

2. A NEW CHANGE ESTIMATOR

The work presented here is closely related to the model and derivation presented in Jakowatz *et al*. [1]. The primary difference between the derivation shown below and that described in [1] is that the simplifying assumption of CNR >> 1 is removed. The final expression for the estimator is surprisingly simple and results in a much more robust estimator in the presence of low image CNR.

We assume we are given two complex SAR images collected at different times. The images are of the same area and collection geometry. We are asked to determine the amount of change that has occurred between the two collects on small sub-patches of the scene. We start with the model:

$$X_{1k} = C_{0k} + n_{1k}$$

$$X_{2k} = \alpha C_{0k} e^{j\varphi} + \left(\sqrt{1 - \alpha^2}\right) C_{1k} + n_{2k} \qquad (3)$$

where X_{1k}, X_{2k}, are the k^{th} complex values of image 1 and image 2 respectively and represent the observed data. α is the change metric we wish to estimate and is defined to be on the interval [0 1] where 0 indicates complete change and 1 represents no change between the collects. The term C_{0k} is the image data that has not changed between collects whereas the term C_{1k} represents the data that has changed between collects. The quantity φ is the constant phase difference that exists between the two images in the local neighborhood of interest. This phase can be caused by terrain topography and/or slight collection geometry differences. This phase term is often exploited to produce very accurate height maps in many two-pass SAR collects, but is of no value to CCD and therefore treated only as a nuisance parameter here. The additive system thermal noise terms are denoted by n_{1k}, and n_{2k}. The local neighborhood is typically a box of size ranging from 3x3 to 9x9 pixels (i.e., 9 to 81 "looks"). These variables are modeled as independent identically distributed (IID) zero mean, Gaussian, random variables with the following relationships:

$$\begin{aligned} E\left\{|C_{0k}|^2\right\} &= E\left\{|C_{1k}|^2\right\} = \sigma_c^2, \\ E\left\{|n_{1k}|^2\right\} &= \sigma_{n1}^2 \\ E\left\{|n_{2k}|^2\right\} &= \sigma_{n2}^2 \ . \end{aligned} \qquad (4)$$

Using the above definitions, we can write

$$E\left\{|X_{1k}|^2\right\} = \sigma_c^2 + \sigma_{n1}^2$$

$$E\{|X_{2k}|^2\} = \sigma_c^2 + \sigma_{n2}^2 . \quad (5)$$

Equation 5 indicates the model ensures the power of X_{1k} and X_{2k} are independent of α.

The above definitions define the data in a local neighborhood of pixels. The model allows the clutter and noise values to change on a neighborhood-to-neighborhood basis. While the clutter value (σ_c^2) represents the image power and does in fact change throughout the scene, the noise term represents thermal noise and therefore can be considered to be constant over the entire image [18].

Rewriting the observations X_{1k} and X_{2k} of Equation 3 in vector form, we have (vectors in bold):

$$X_k = \begin{bmatrix} X_{1k} \\ X_{2k} \end{bmatrix} = C_{0k}\begin{bmatrix} 1 \\ \alpha e^{j\varphi} \end{bmatrix} + C_{1k}\begin{bmatrix} 0 \\ \sqrt{1 - \alpha^2} \end{bmatrix} + \begin{bmatrix} n_{1k} \\ n_{2k} \end{bmatrix} \quad (6)$$

and the covariance matrix Q is:

$$Q = E\{X_k X_k^H\} = \begin{bmatrix} \sigma_c^2 + \sigma_{n1}^2 & \alpha\sigma_c^2 e^{-j\varphi} \\ \alpha\sigma_c^2 e^{j\varphi} & \sigma_c^2 + \sigma_{n2}^2 \end{bmatrix} . \quad (7)$$

The superscript H indicates the complex conjugate transpose (Hermitian) operation. Invoking the mutual independence of the observations, we can write a joint conditional density function that is given by:

$$P(X \mid \varphi,\alpha) = \frac{1}{\pi^{2N}|Q|^N} e^{-\sum_{k=1}^{N} X_k^H Q^{-1} X_k} . \quad (8)$$

The maximum likelihood (ML) estimate of α is the value of α that maximizes Equation 8, or equivalently the log of Equation 8. We treat the phase term φ as an unknown nuisance parameter and use its ML estimate in the derivation [1]. The estimate is found by taking the derivative of the log of Equation 8, setting the result to zero and solving for α.

The log of Equation 8 is easily shown to be

$$\ln\{P(X \mid \varphi,\alpha)\} = -2N\ln\pi - N\ln|Q| - \sum_{k=1}^{N} X_k^H Q^{-1} X_k . \quad (9)$$

Taking the partial derivative of Equation 8 with-respect-to α and setting the result to zero gives

$$\sum_{k=1}^{N} \{X_k^H [\frac{d}{d\alpha}(Q_c)|Q|^{-1} - Q_c|Q|^{-2}\frac{d}{d\alpha}(|Q|)]X_k\} - N\frac{\frac{d}{d\alpha}(|Q|)}{|Q|} = 0 \quad (10)$$

where $Q^{-1} = \frac{Q_c}{|Q|}$. In this case $Q_c = \begin{bmatrix} \sigma_c^2 + \sigma_{n1}^2 & -\alpha\sigma_c^2 e^{-j\varphi} \\ -\alpha\sigma_c^2 e^{j\varphi} & \sigma_c^2 + \sigma_{n2}^2 \end{bmatrix}$ and $|Q| = \left(\sigma_c^2 + \sigma_{n1}^2\right)^2 - \alpha^2\sigma_c^4$.
Substituting the above definitions into Equation 10 and replacing φ with its maximum-likelihood estimate, $\varphi_{ML} = \angle\left\{\sum_{k=1}^{N} X_{1k}^* X_{2k}\right\}$ (see [1]), we have, after a considerable amount of algebraic manipulation, the following cubic equation:

$$\left(\alpha - \frac{\left|\sum_{k=1}^{N} X_{1k}^* X_{2k}\right|}{N\sigma_c^2}\right)\left(\alpha^2 + AB\right) = 0 \quad , \tag{11}$$

where $A = \frac{\sigma_c^2 + \sigma_{n1}^2}{\sigma_c^2}$ and $B = \frac{\sigma_c^2 + \sigma_{n2}^2}{\sigma_c^2}$. The only viable solution is:

$$\alpha_{ML} = \frac{\left|\sum_{k=1}^{N} X_{1k}^* X_{2k}\right|}{N\sigma_c^2} \tag{12}$$

because the other two roots of this equation are not real. The above expression requires knowledge of σ_c^2 in each local neighborhood. This value can be approximated from the measured data of the detected radar image in that neighborhood. Using the relationships in Equation 5 we have:

$$E\left\{|X_{1k}|^2\right\} = \sigma_c^2 + \sigma_{n1}^2 \approx \frac{\sum_{k=1}^{N} |X_{1k}|^2}{N}$$

$$E\left\{|X_{2k}|^2\right\} = \sigma_c^2 + \sigma_{n2}^2 \approx \frac{\sum_{k=1}^{N} |X_{2k}|^2}{N} \quad . \tag{13}$$

The two equations above can be combined to produce an estimate of σ_c^2 giving:

$$\sigma_c^2 \approx \frac{\sum_{k=1}^{N} |X_{1k}|^2 + \sum_{k=1}^{N} |X_{2k}|^2 - N\sigma_{n1}^2 - N\sigma_{n2}^2}{2N} \quad . \tag{14}$$

Substituting Equation 14 into Equation 12, we can write the closed-form solution

$$\alpha_{ML} = \frac{2\left|\sum_{k=1}^{N} X_{1k}^{*} X_{2k}\right|}{\left(\sum_{k=1}^{N} |X_{1k}|^2 + \sum_{k=1}^{N} |X_{2k}|^2 - N\sigma_{n1}^2 - N\sigma_{n2}^2\right)}. \quad (15)$$

The new ML change estimate given by Equation 15 collapses to Equation 1 if CNR >> 1 and $\sum_{k=1}^{N} |X_{1k}|^2 \approx \sum_{k=1}^{N} |X_{2k}|^2$.

[This page intentionally blank]

3. IMPLEMENTATION

The model we use in this derivation assumes the clutter power in a particular neighborhood is equal in both images and is defined as σ_c^2. This value changes from neighborhood-to-neighborhood as it represents the scene reflectivity. The model allows the noise terms to be

different in the two images (σ_{n1}^2 and σ_{n2}^2). This could be caused from a variety of reasons such as differing collect slant ranges.

Before applying the new estimation technique, one must ensure that the average reflectivities in the two images are approximately equal and have knowledge of the noise power in both images. One can always ensure that the average reflectivity is approximately the same in both images by simply scaling one image by a constant. The needed constant scale factor and the two image noise powers may be known *a priori* from the system design and image formation specifications. If these quantities are not known, we propose the following procedure to assure that the unknown thermal noise values are properly measured and the clutter in the two images is approximately the same.

1) Make four image measurements $\bar{P}_{m1}$, $\bar{P}_{m1}$, $\bar{\sigma}_{mn1}^2$, and $\bar{\sigma}_{mn2}^2$. The *m* in the subscripts denotes that these are measured values and the bar over the variables indicate they are image average values. The measurements are obtained as:

   $\bar{P}_{m1}$: Average power in image 1. This is the measured clutter power plus noise power in image 1:

   $$\bar{P}_{m1} = \bar{\sigma}_{mc1}^2 + \bar{\sigma}_{mn1}^2$$

   $\bar{P}_{m2}$: Average power in image 2. This is the measured clutter power plus noise power in image 2:

   $$\bar{P}_{m2} = \bar{\sigma}_{mc2}^2 + \bar{\sigma}_{mn2}^2$$

   $\bar{\sigma}_{mn1}^2$ and $\bar{\sigma}_{mn2}^2$: The measured noise values for images 1 and 2. These values can be measured in a shadow region of the image. Our goal is to measure only the thermal noise term as it can be considered to be constant throughout the scene [2]. Using this approach, care must be taken to avoid including multiplicative noise in the measurement. This can be done by avoiding shadow/clutter boundary regions when the measurement is done.

2) Scale image 2 by the factor: $\gamma = \sqrt{\dfrac{\bar{P}_{m1} - \bar{\sigma}_{mn1}^2}{\bar{P}_{m2} - \bar{\sigma}_{mn2}^2}}$. This ensures that the average clutter values in both images are the same and set to: $\bar{\sigma}_c^2 = \bar{P}_{m1} - \bar{\sigma}_{mn1}^2$.

3) Use the quantities: $\sigma_{n1}^2 = \bar{\sigma}_{mn1}^2$, and $\sigma_{n2}^2 = \gamma^2 \bar{\sigma}_{mn2}^2$ to calculate α_{ML} in Equation 15.

The output of the traditional estimator (Equation 1) is constrained α to lie in the interval [0 1]. In general the output of the new estimator in Equation 15 does remain in the [0 1] interval. However, in some situations such as completely shadowed regions, the denominator of Equation 15 can become quite small and the resulting output may be well outside these bounds. This can be dealt with in a number ways. One approach is to flag these areas as regions where the change

estimate is unreliable due to low clutter power. For the results in this paper, we address this by setting α to be 1 if the result is outside the [0 1] interval.

4. SYNTHETIC DATA EXAMPLE

We next show two examples using simulated data that illustrate the deficiencies of the traditional estimator of Equation 1 and how the new estimator of Equation 15 mitigates these shortcomings. The synthetic examples serve to illustrate the true nature of the estimator in a controlled environment.

The detected images of the first synthetic example are shown in Figure 1. Both images were generated using random Gaussian complex numbers according to the model in Equation 3. Both

images contain a vertical strip on the left side of the image that simulates a lower return than the rest of the image. This region represents a road in a real image that has lower return. The power in this area is 5 times lower than the power in the rest of the image. The data in this region is the same in both images ($\alpha = 1$ in Equation 3) so an ideal estimator should produce an estimate of 1 in this area. Another strip on the right side of the second image was generated with $\alpha = 0$ which represents a true change between images. The data in this strip has the same power as the data surrounding it so this true change area is largely undetectable in the detected images shown in Figure 1. Different realizations of random Gaussian noise were added to both images to satisfy Equation 3. The power of the noise was identical to the power in the low-return vertical stripe on the left of the images bringing the CNR in that area to be 0dB.

The results of the original CCD estimator of Equation 1 and the new CCD estimator of Equation 15 with both using a 7x7 pixel box (49 looks) are shown in Figure 2. An ideal estimator would produce $\alpha=1$ everywhere except the right strip where the result would be zero. The result of the traditional CCD estimator is shown in the left side of Figure 2. Note that both the left and the right strip do show loss of coherence. The left strip has undesirable coherence loss because of low CNR, while the right strip decorrelates because it simulates an area of true physical change. The result of the new CCD estimator is on the right. Note the general improvement of coherence over the entire scene. The left strip coherence is near unity, even with the low CNR, and the right strip shows coherence loss due to true change. The average coherence for both techniques is shown in plots below the respective CCD results. These plots were generated by averaging the CCD results in the vertical direction.

The purpose of the second synthetic example is to illustrate a situation where the traditional estimator can mask a true change that has occurred (a “missed detection”). The detected images of the second synthetic example are shown in Figure 3. In this example a simulated road going vertically is placed in the center of both images (lower-return area). Simulated vehicle tracks are inserted in the center of the road in the second (post) image. The vehicle tracks are the ‘true change’ that we want to detect. Both images were generated using random Gaussian complex numbers according to the model in Equation 3. The power in the road is 5 times lower than the power in the rest of the image. The data in the road region is the same in both images ($\alpha = 1$ in Equation 3). The vehicle tracks are realized by two vertical strips (5 pixels wide and 30 pixels apart) in the center of the road in the second image. The vehicle track strips are generated using the relationship in Equation 3 where for each pixel, α was randomly set to 0 or 1. This attempts to simulate the decorrelation a tire track causes in dirt road. Different realizations of random Gaussian noise were added to both images to satisfy Equation 3. The power of the noise was identical to the power in the road area bringing the CNR in that area to be 0dB.

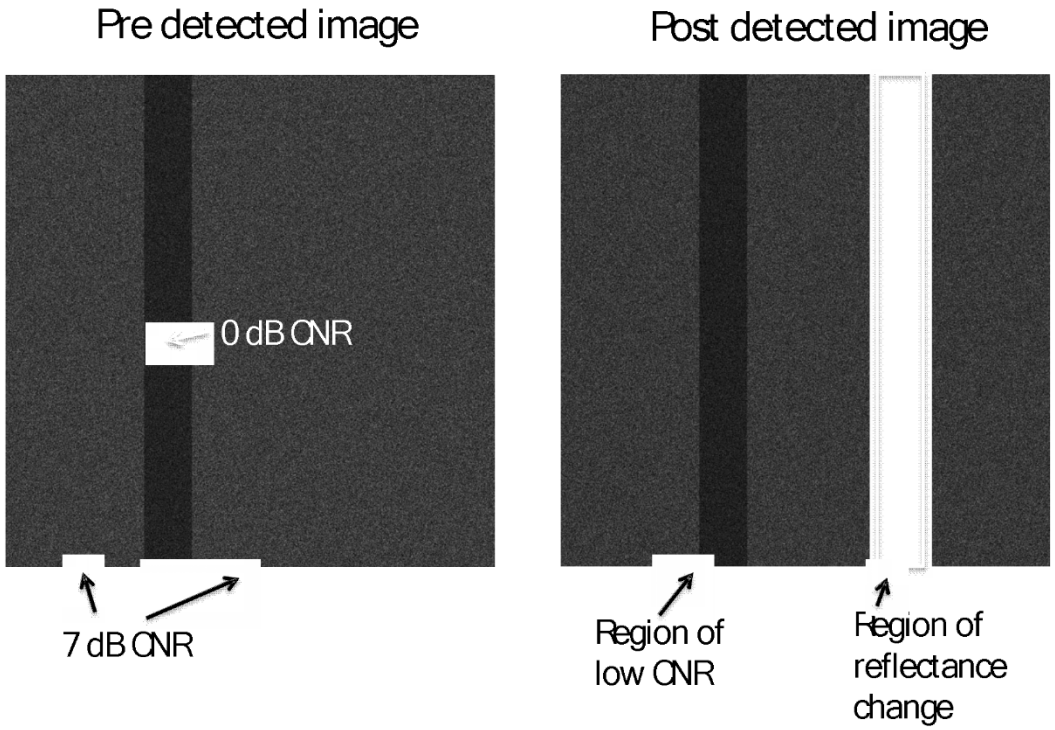

Figure 1. Two synthetic images were generated using random Gaussian complex numbers according to the model in Equation 3. The vertical strip on the left side of both images had 5 times less power than the rest of the image. Different realizations of noise were added to each image with the same power as that of the lower power vertical strip on the left giving a 0 dB level of CNR in that area. The alpha value was set to 1 for most of the image except the vertical strip on the right. In that region it was set to 0.

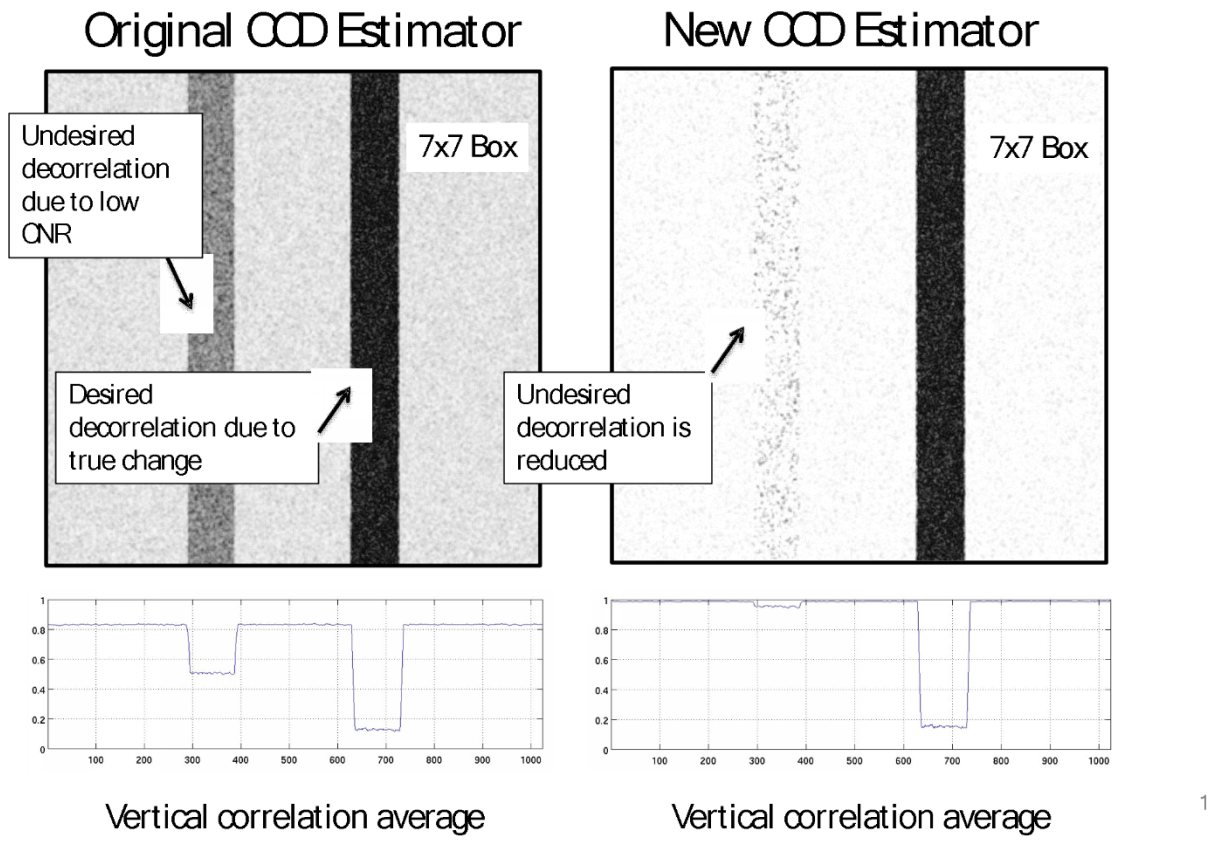

Figure 2. The CCD results of the two synthetic images shown in Figure 1. The left is the result of the traditional CCD operation (Equation 1). The right shows the result of the new CCD estimator calculated using Equation 15. The plots below both CCD results are the average of the CCD values in the vertical direction. Note the average value of the new CCD estimator is increased in areas that have no true change while the area that does have true change (the vertical strip on the right) remains approximately the same.

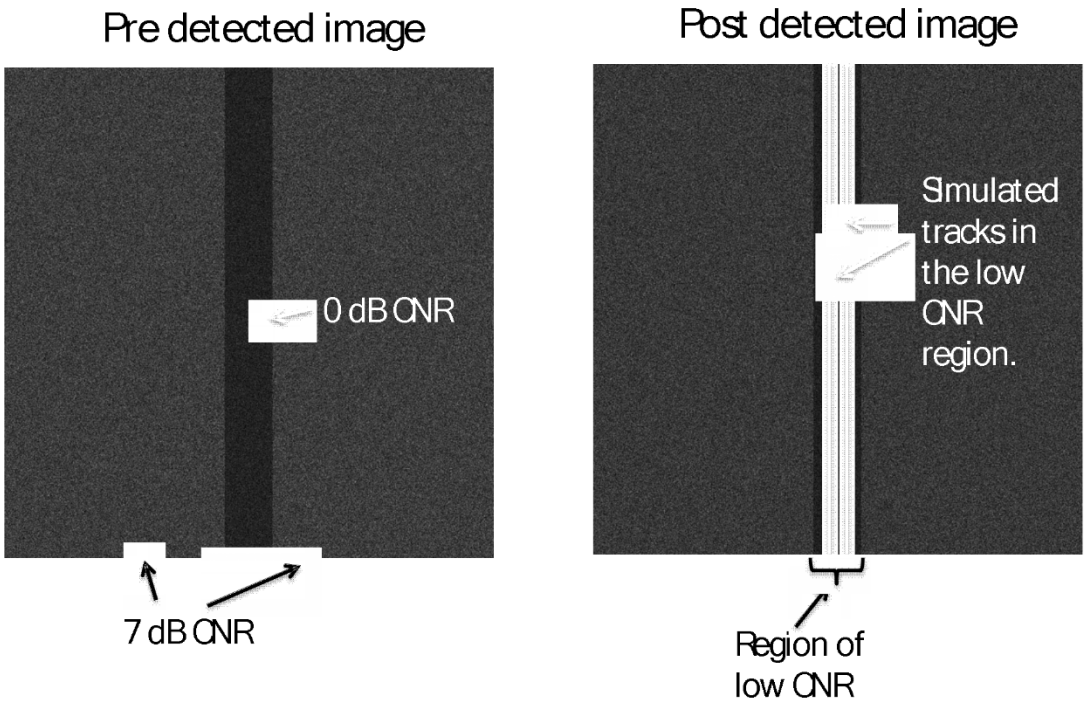

Figure 3. Two synthetic images were generated using random Gaussian complex numbers according to the model in Equation 3. The vertical strip in the center of both images had 5 times less power than the rest of the image. Simulated vehicle tracks were added to the post image on the right. The power of the track data was identical to the power of the center stripe making it difficult to see in the detected image. The tracks had an axle width of 30 pixels and a tire width of 5 pixels. The data in the tire track region was generated using the model in Equation 3 where for each pixel in the track, alpha was randomly set to either 0 or 1. This is intended to represent realistic tire track disturbance. Different realizations of noise were added to each image with the same power as that of the lower power vertical strip on the left giving a 0 dB level of CNR in that area.

The results of the original CCD estimator of Equation 1 and the new CCD estimator of Equation 15 using a 7x7 pixel box or 49 looks are shown in Figure 4. The result of the traditional CCD estimator is shown in the left side of Figure 4. Note that the vehicle tracks, although visible, are difficult to detect because of the false decorrelation produced by low return of the road itself. The result of the new CCD estimator is on the right. Note the general improvement of correlation over the entire scene. The decorrelation due to the low return of the road is greatly improved leaving the 'true change' caused by the tracks much more obvious. The average

decorrelation for both techniques is shown in plots below the respective CCD results. These plots were generated by averaging the CCD results in the vertical direction. Note the increased level of discrimination between the "road" and the simulated vehicle tracks by comparing the traditional CCD estimator results to the new CCD estimator. Not only does the new CCD estimator raise the surrounding "no change", low-CNR road CCD value from approximately 0.50 to 0.96, it increases the difference between the no change value and vehicle track change value from approximately $\Delta\alpha = 0.12$ (0.50 – 0.38) in the traditional CCD result to approximately $\Delta\alpha = 0.21$ (0.96 – 0.75) in the new CCD results as shown in Figure 4's graphs.

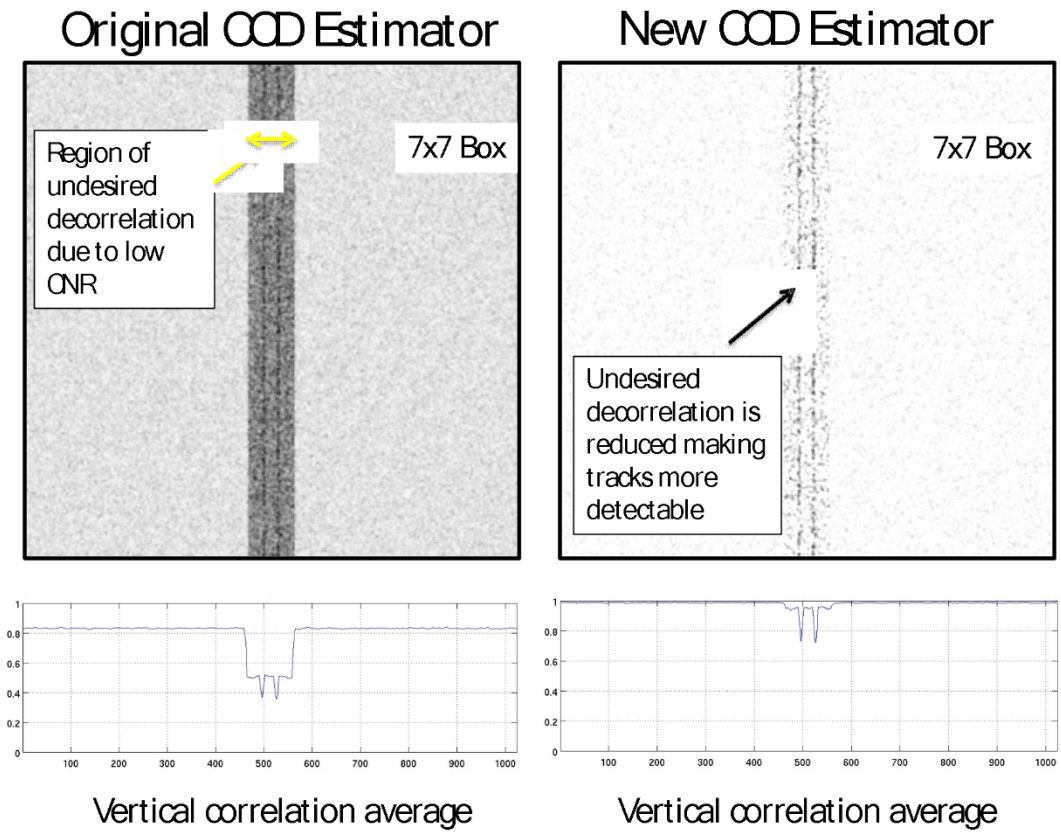

Figure 4. The CCD results of the two synthetic images shown in Figure 3. The left is the result of the traditional CCD operation (Equation 1). The right shows the result of the new CCD estimator calculated using Equation 15. The plots below both CCD results are the average of the CCD values in the vertical direction. Note the vehicle tracks in the right image are more pronounced than those in the left image making them much more likely to be detected.

[This page intentionally blank]

5. REAL DATA EXAMPLE

The new detection algorithm was used on an example set of SAR images taken in a remote area with several dirt-packed roads. The data was collected by an airborne X-band system designed and operated by Sandia National Laboratories. The detected image from one of the collects is shown in Figure 5. A vehicle was driven from the top to the bottom on the far-right road. It travelled out of the scene and back in the scene on a road on the left of the image. This vehicle movement happened between the two radar collections. Figure 6 shows the resulting change map using the traditional change estimator of Equation 1. Note that the roads in the "tick-tack-toe" array, which were not traveled upon between collections, appear to have some decorrelation simply because of the relatively low microwave reflectivity of the smooth road. Use of the traditional change estimator (Equation 1) makes it difficult to determine if the road on the right is decorrelated due to lower CNR or if a single vehicle or many vehicles actually travelled it. Figure 7 shows the change map using the new CCD estimator of Equation 15. Note that the detectability of a single vehicle traveling on the road to the right is dramatically improved. Using the traditional CCD estimation scheme, the road itself is decorrelated due to low CNR and was masking the true decorrlation caused by the vehicle tires. The CNR on the road area was measured to be approximately 0dB. This is a situation very similar to the second synthetic example shown in Figures 3-4. In addition, the ambiguities of the " tick-tack-toe " untraveled roads are removed. The small horizontal shadow strip in the right of the image was used to calculate the image noise terms.

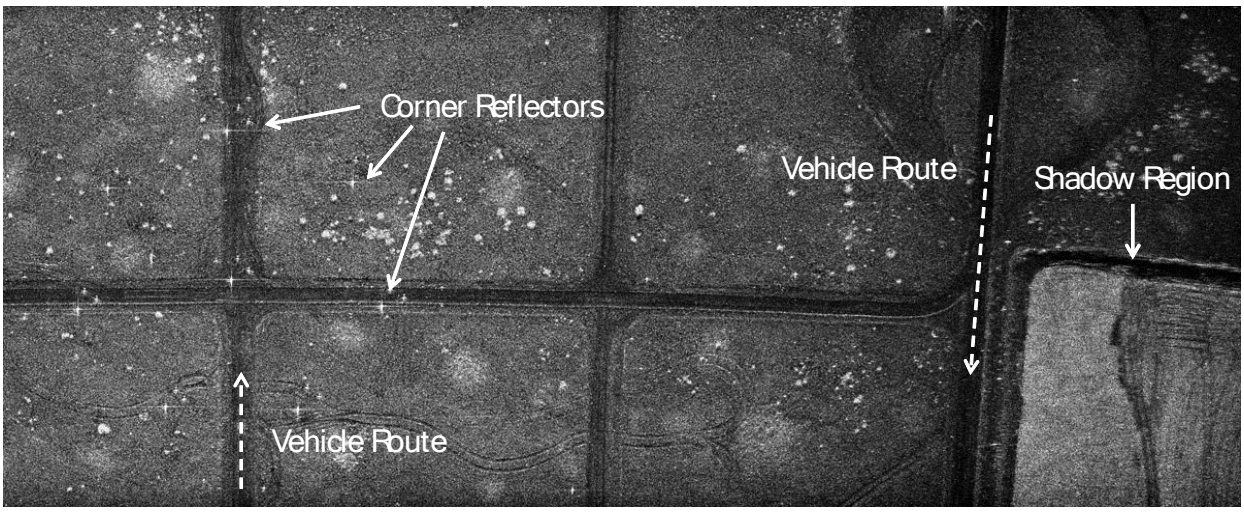

Figure 5. Detected image from the first of two airborne SAR collects. The two images form a SAR coherent pair of images. A vehicle traveled on the vertical road on the right side of the scene as well as on a portion of one of the vertical roads in the "tick-tack-toe " array on the left side of the image. The scene contains some corner reflectors placed in a circle on the left side of the scene

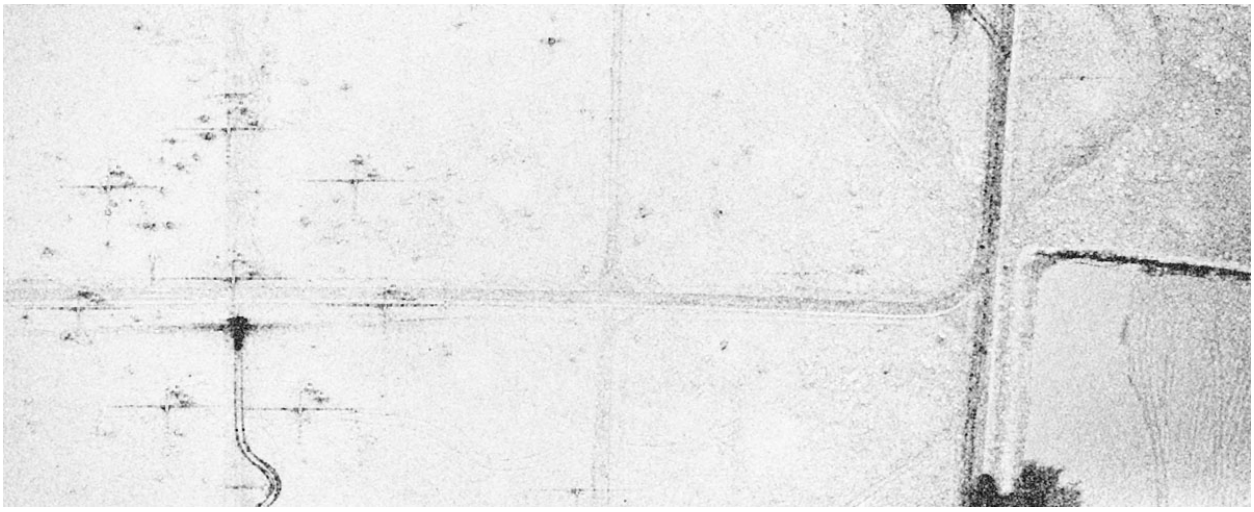

Figure 6. Resulting coherent change map using the traditional detector shown in Equation 1 using a box size of 7x7 pixels. Note that most of the untraveled roads of the "tick-tack-toe" array appear to have some decorrelation. It is difficult to discern if the decorrelation on many of the roads is due to true change or is simply the result of the low CNR. The corner reflectors also have some decorrelation caused by phenomenon not addressed in this paper.

Figure 7. Change map of new method using Equation 15 using a box size of 7x7 pixels. Note the much improved detectability of the vehicle tracks going from top to bottom on the right side of the image. These tracks were essentially masked using the old CCD estimator (Figure 6) since they resided on the low CNR road area. Note that the new CCD estimator also removes the low correlation of many of the packed-untraveled road surfaces, leaving the true change information.

6. FUTURE WORK

The derivation of the ML change estimate in Equation 15 assumes we have two SAR collects of the same area with the same collection geometry. These collects were done with the same polarization. The formulation of the probability distribution in Equation 8 lends itself to extending the change estimator for multi-polarization SAR collects. Also, an in-depth analysis of the statistical performance of the single polarization and a possible multi-polarization temporal ML change estimate is in order.

[This page intentionally blank]

7. CONCLUSION

Temporal decorrelation in repeat-pass, repeat-geometry interferometric SAR imagery pairs can detect changes in the complex reflection caused by vehicles, animal, and human traffic. However, the change metric generally used for CCD, and presented in Equation 1, is a maximum likelihood (ML) change estimate in a very limited sense. Using the Equation 1 change metric, real-world SAR CCD products exhibit decorrelation/temporal change results for low CNR targets or areas when there is actually no temporal change. Therefore, a new ML change estimator was derived incorporating changing CNR levels (Equation 15). The resulting estimator is simple in form and easy to implement. The new ML estimated CCD was calculated for both simulated and actual SAR imagery demonstrating reduction of false-change results (false alarms) compared to the Equation 1 change estimate, while preserving and improving the differentiation between change and no change, (see Figure 4).

[This page intentionally blank]

8. REFERENCES

1. C. V. Jakowatz Jr., D. E. Wahl, P. H. Eichel, D. C. Ghiglia and P. A. Thompson, Spotlight-mode Synthetic Aperture Radar: A Signal Processing Approach, Boston: Kluwer Academic Publishers, 1996.
2. L. Graham, "Synthetic interferometer RADAR for topographic mapping," in *Proceedings of the IEEE, vol. 62, no. 6, pp. 763-768*, 1974.
3. H. A. Zebker and R. M. Goldstein, "Topographic mapping from interferometric synthetic aperture radar observations," *Journal of Geophysical Research,* vol. 91, no. B5, pp. 4993-4999, 1986.
4. A. K. Gabriel and R. M. Goldstein, "Cross orbit interferometry - Theory and experimental results from SIR-B," *International Journal of Remote Sensing,* vol. 9, no. 5, pp. 857-872, 1988.
5. F. Li and R. M. Goldstein, "Studies of multi-baseline spaceborne interferometric synthetic aperture radars," *IEEE Transactions on Geoscience and Remote Sensing,* vol. 28, no. 1, pp. 88-97, 1990.
6. E. Rodriquez and J. M. Martin, "Theory and design of interferometric synthetic aperture RADARs," *IEE Proceedings-F,* vol. 139, pp. 147-159, 1992.
7. A. L. Gray and P. J. Farris-Manning, "Repeat-pass interferometry with airborne synthetic aperture RADAR," *IEEE Transactions on Geoscience and Remote Sensing,* vol. 31, no. 1, pp. 180-191, 1993.
8. D. Massonnet, M. Rossi, C. Carmona, F. Adragna, G. Peltzer, K. Feigl and T. Rabaute, "The displacement field of the Landers earthquake mapped by RADAR interferometry," *Nature,* vol. 364, no. 6433, pp. 138-142, 1993.
9. M. Born and E. Wolf, Principles of Optics, Sixth Edition, New York: Pergamon Press, 1984.
10. H. A. Zebker and J. Villasenor, "Decorrelation in interferometric radar echoes," *IEEE Transactions on Geoscience and Remote Sensing,* vol. 30, no. 5, pp. 950-959, 1992.
11. D. G. Corr and A. Rodrigues, "Coherent change detection of vehicle movements," in *IEEE International Geoscience and Remote Sensing*, Seattle, 1998.
12. D. A. Yocky and B. F. Johnson, "Repeat-pass dual-antenna synthetic aperture radar interferometric change detection post processing," *Photogrammetric Engineering and Remote Sensing,* vol. 64, no. 5, pp. 425-429, 1998.
13. D. Just and R. Bamler, "Phase statistics of interferograms with applications to synthetic aperture radar," *Applied Optics,* vol. 33, no. 20, pp. 4361-4368, 1994.
14. R. Touzi, A. Lopes, J. Bruniquel and P. W. Vachon, "Coherence estimation for SAR imagery," *IEEE Transactions on Geoscience and Remote Sensing,* vol. 37, no. 1, pp. 135-149, 1999.
15. J. Barber and S. Kogon, "Probabilistic three-pass SAR coherent change detection," in *2012 Conference Record of the Forty Sixth Asilomar Conference on Signals, Systems and Computers*, Pacific Grove, Nov, 2012.
16. M. A. Preiss, D. A. Gray and N. J. S. Stacy, "Detecting scene changes using synthetic aperture radar interferometry," *IEEE Transactions on Geoscience and Remote Sensing,* vol. 44, no. 8, pp. 2041-2054, 2006.
17. M. Newey, J. Barber, G. Benitz and S. Kogon, "False alarm mitigation techniques for SAR CCD," in *IEEE Radar Conference*, Ottawa, 2013.

18. W. G. Carrara, R. S. Goodman and R. M. Majewski, "8.4.2 Additive Noise," in *Spotlight Synthetic Aperture Radar*, Boston, Artech House Publishers, 1995, pp. 333-335.

DISTRIBUTION

4 Dr. Victoria Franques
Program Manager, Office of Proliferation Detection Program
Defense Nuclear Nonproliferation Research and Development
National Nuclear Security Administration
U.S. Department of Energy, NA-22
1000 Independence Ave. SW
Washington, D.C. 20585

1	MS0519	Steven Castillo	5349
1	MS0519	James G. Chow	5349
1	MS0533	Robert Riley	5342
1	MS0968	Robert D. M. Tachau	5753
1	MS0980	Jeffrey A. Mercier	5772
1	MS1207	Charles V. Jakowatz, Jr.	5962
5	MS1207	Daniel E. Wahl	5962
1	MS1207	David A. Yocky	5962
1	MS1209	John E. Gronager	5960
1	MS0899	Technical Library	9536 (electronic copy)

[This page intentionally blank]


Sandia National Laboratories